Quadrupolar Order Shimming of Permanent Magnets Using Harmonic Corrector Rings

R. C. Jachmann,[1] D. R. Trease,[1] L.-S. Bouchard,[1] D. Sakellariou,[2]
R. W. Martin,[3] R. D. Schlueter,[4] T. F. Budinger,[5] and A. Pines[1]

[1]*Materials Sciences Division, Lawrence Berkeley National Laboratory,*
Berkeley, California 94720 and Department of Chemistry,
University of California, Berkeley, California 94720
[2]*Laboratoire de Structure et Dynamique par Résonance Magnétique, Commissariat à l'Énergie Atomique,*
Service de Chimie Moléculaire, CEA Saclay, Gif-sur-Yvette, France, 91191
[3]*Department of Chemistry, University of California, Irvine, California 92697*
[4]*Engineering Division, Lawrence Berkeley National Laboratory, Berkeley, California 94720*
[5]*Life Sciences Division, Lawrence Berkeley National Laboratory, Berkeley, California 94720*
(Dated: October 30, 2006)

Shimming systems are required to provide sufficient field homogeneity for high resolution NMR. In certain specialized applications, such as rotating-field NMR and portable (ex-situ) NMR, permanent magnet-based shimming systems can provide considerable advantages. We present a simple two-dimensional shimming method based on harmonic corrector rings which can provide arbitrary multipole order shimming corrections. Results demonstrate, for example, that quadrupolar order shimming improves the linewidth by up to an order of magnitude. An additional order of magnitude reduction is in princliple achievable by ultilizing this shimming method for z-gradient correction and higher order xy gradients.

I. INTRODUCTION

Magnet shimming is an essential part of NMR spectroscopy. Removing inhomogeneities arising from magnet design and contruction should be done to the best extent possible in order to allow resolution of spectroscopic peaks. If left uncorrected field inhomogeneities obsure chemical shielding information needed to provide structural detail.

This is particularly relevant when designing a portable NMR apparatus. These small scale magnets are fabricated using a small number of permanent magnet (PM) blocks or coils. The resulting field is highly inhomogeneous by NMR standards. Based on our experience, a 16-element Halbach array designed to create a dipole field can easily exhibit inhomogeneities upwards of 500 parts per million (ppm) over cubic millimeter volumes, which is unacceptable for high-resolution spectroscopy. Though more homogeneous arrays have been created showing inhomogeneities of 100ppm and even as low as 20ppm[1,2] there is still a need for shimming systems.

Magnetic fields, and consequently the their field inhomogeneities obey Maxwell's equations. Therefore, a shimming scheme capable of producing an arbitrary 3-D perturbation field can in principle null, that is cancel out, any concievable preexisting inhomogeneity. The standard method of shimming an NMR magnet utilizes an expansion of the magnetic field in spherical harmonics. Since the magnetic scalar potential obeys the Laplace equation $\nabla^2 \Phi_M = 0$ and the magnetic field is the gradient of this potential $\mathbf{H} = \nabla \Phi_M$, differentiation of the Laplace equation reveals that each component of the magnetic field also obeys the Laplace equation. In particular, we have $\nabla^2 H_z = 0$. This permits an expansion of the field in terms of spherical harmonics[3]:

$$
\begin{aligned}
H_z(\mathbf{r}) - H_z(0) &= \sum_{l=1}^{\infty} \left(\frac{4\pi}{2l+1} \right)^{1/2} r^l \sum_{m=-l}^{+l} a_{lm} Y_{lm}(\Theta, \Phi) \\
&= a_{10}z - \Re a_{11}\sqrt{2}x + \Im a_{11}\sqrt{2}y \\
&\quad + a_{20}\frac{2z^2 - r^2}{2} + \Re a_{22}\sqrt{\frac{3}{2}}(x^2 - y^2) \\
&\quad + \sqrt{6}(\Im a_{21}yz - \Re a_{21}xz - \Im a_{22}xy) + \dots
\end{aligned}
$$
(1)

where $a_{l,-m} = (-1)^m a_{lm}^*$, thus making the field real-valued. Because H_z is much larger than the transverse components, H_x or H_y, they are truncated by H_z and therefore negligible. Hence, to a good approximation, H_z determines the Larmor frequency. The task of the shimming system is to vary the currents in shim coils, which amounts to varying the coefficients $\Re a_{lm}$ or $\Im a_{lm}$.

Similarly, spherical harmonics can be used when the shims are Halbach-type arrays instead of coils, however the solution and execution are of slightly different form. Halbach-type arrangements can provide one-sided fluxes which show a remarkable degree of uniformity inside a ring and nearly zero flux outside[4]. This means the usable shimming field can be relatively large; in fact, almost as large as the shimming aperture itself. Additionally, the absence of flux outside the aperture does not perturb the magnet creating the external field. While shim coils can achieve considerable homogeneity over the bore Halbach-

type shimming can have its advantages in smaller systems. When designing small scale portable magnets with small bores, it is crucial that the shimming system does not occupy too much space inside the bore of the magnet, as this would severely limit the usable region. In these smaller systems the Halbach-type arangement can have a significant strength superiority to the shimming coil and still be considerably compact leaving a large bore size available and still retain it's harmonic tunability capabilities. Futhermore, Halbach arrays eliminate the need for a power supply, which can be important in portable "ex-situ" and rotating field type sytems. Fulfilling the need for a shimming systems suited for rotating field NMR systems[5,6] would be technically challenging in connecting and controling electro-coil shims as the shimming coils would need to rotate with the field. However permanent magnets supply a perfect solution as they have no leads which would tangle as the bore rotates.

To overcome these difficulties, in the contexts of portable and/or rotating field NMR systems, we present a "one shot" shimming system where one maps the field and compensates for each order of inhomogeneity in the field. Shimming with this method can be done in real time, using field mapping, or it can be done only once, as part of the magnet design phase.

The novelty of our method lies in its use of harmonic corrector rings[7] which are rings composed of concentric permanent magnet rods (magnetic dipoles) whose overall and relative orientations can be used to adjust the field strength, orientation, and multipole order. In our case, the rods are substituted by adjacent pairs of small disc permanent magnets(PMs) which approximate magnetic dipoles. We demonstrate its implementation in generating quadrupolar fields to correct inhomogeneities. Any number of additional rings can be added to correct arbitrary multipole orders simultaneously.

II. THEORY

A. General multipole correction

Magnets can be arranged in a ring to produce a field of a chosen order, N, by careful control of their overall and relative orientations. Assembled this way they can be used to correct for an inhomogeneity in an already existing magnetic field. In order to null a multipole term of order N, using a single ring of equally spaced magnets as in Figure 1, the orientation of the nth magnet is given by[7]:

$$\phi_n = (N+1)\beta_n + \phi_{init} \tag{2}$$

where β_n is the angle of the location of the nth magnet on the ring and ϕ_{init} is an angle defined, with respect to the x axis, by the orientation of the required multipole. In general, the magnetic dipole moment of the nth magnet
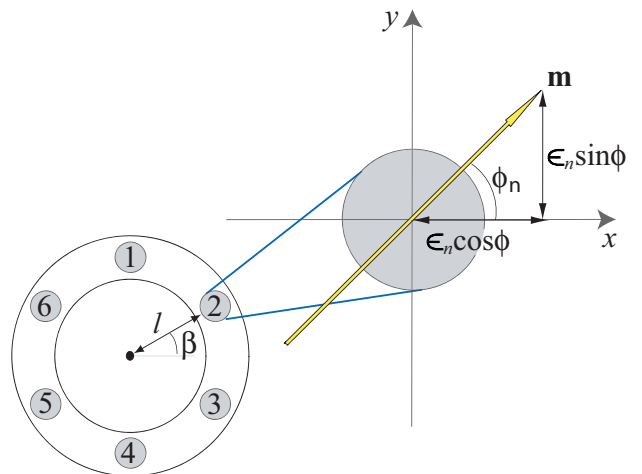

FIG. 1: The magnets 1 to 6 have β_n values $\pi/2$, $\pi/6$, $11\pi/6$, $3\pi/2$, $7\pi/6$, $5\pi/6$.
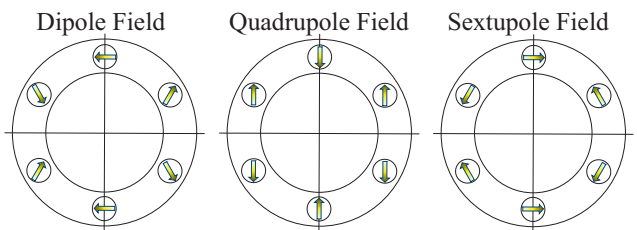

FIG. 2: A ring of 6 magnets oriented to produce a dipole, quadrupole, and sextupole field. These orientations are based on Equation 2. The quadrupole arrangement can be used to null a gradient in a strong magnetic field; to control the strength of the gradient, additional rings are necessary.

is given by $\mathbf{m}_n = \epsilon_n(\cos\phi_n, \sin\phi_n, 0)$, where ϵ_n is its strength.

Figure 2 shows a ring of six magnets oriented to produce dipolar, quadrupolar and sextupolar magnetic fields in this manner.

B. Quadrupolar correction

Our analysis will concentrate on the quadrupolar case, though extension to higher orders is straightforward (see Appendix). In this case, $N = 2$ and ϕ_{init} is the orientation of the H_x component of the quadrupole. Using β_n values defined for a six-magnet ring in Figure 1 and applying these values to Equation 2, we get:

$$\phi_o = \phi_e + \pi = \phi_{init} + \frac{3\pi}{2} \tag{3}$$

where ϕ_o is the orientation of odd-numbered magnets and ϕ_e is the orientation of the even-numbered magnets. Thus, going round the circle, the orientation of neighboring magnets differs by π. In order to control the magnitude and orientation of the quadrupole, we analyzed
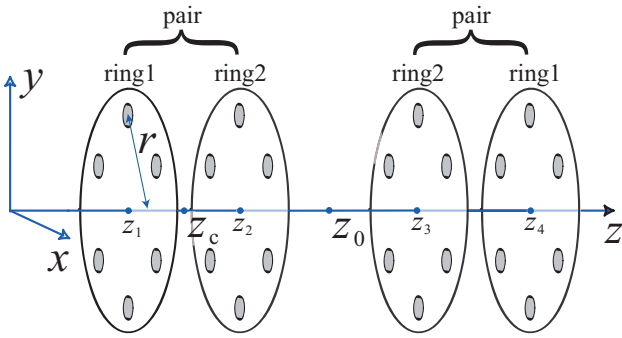
FIG. 3: Spatial arrangement of the ring pairs. The analysis is limited to points along the z-axis, which runs through the center of the two ring pairs.

TABLE I: The position and magnetic dipole moment vectors for the magnets as shown in Figure 1. The ring is determined by the index on z.

| | r | | | m/ϵ | | |
	r_x	r_y	r_z	m_x	m_y	m_z
1	0	$-l$	$-z_i$	$\cos\theta$	$\sin\theta$	0
2	$-\sqrt{3}l/2$	$-l/2$	$-z_i$	$\cos(\theta+\pi)$	$\sin(\theta+\pi)$	0
3	$-\sqrt{3}l/2$	$l/2$	$-z_i$	$\cos\theta$	$\sin\theta$	0
4	0	l	$-z_i$	$\cos(\theta+\pi)$	$\sin(\theta+\pi)$	0
5	$\sqrt{3}l/2$	$l/2$	$-z_i$	$\cos\theta$	$\sin\theta$	0
6	$\sqrt{3}l/2$	$-l/2$	$-z_i$	$\cos(\theta+\pi)$	$\sin(\theta+\pi)$	0

the contribution of each magnet and magnet ring to the overall magnetic field.

If the dimensions of a magnet are small in comparison to the distance to a point, $\mathbf{r}$, at which a field measurement is being made, then the magnet can be approximated as a point dipole. The magnetic field of a point dipole at $\mathbf{r}$ is given by:

$$\mathbf{H}(\mathbf{r}) = \frac{1}{4\pi r^3}\left[3(\mathbf{m}\cdot\hat{\mathbf{r}})\hat{\mathbf{r}} - \mathbf{m}\right] \quad (4)$$

where $\mathbf{H} \equiv (H_x, H_y, H_z)$ is the magnetic field at $\mathbf{r}$, the position vector of the measurement point relative to the position of the dipole. Differentiation of this expression with respect to $\mathbf{r}$ gives the field gradient due to the point dipole:

$$\frac{d\mathbf{H}}{d\mathbf{r}} = \frac{3}{4\pi r^4}\left[\mathbf{m}\otimes\hat{\mathbf{r}} + \hat{\mathbf{r}}\otimes\mathbf{m} + (\mathbf{m}\cdot\hat{\mathbf{r}})\mathbf{I} - 5(\mathbf{m}\cdot\hat{\mathbf{r}})(\hat{\mathbf{r}}\otimes\hat{\mathbf{r}})\right] \quad (5)$$

where $\mathbf{I}$ is the identity tensor.

In our experiments, the x axis was designated as main magnetic field direction, while the z direction was along the longitudinal axis of the magnet bore. Truncation of H_y and H_z, as described in the introduction, means that the relevant tensor component for our experiments is $dH_x/d\mathbf{r}$.

We now restrict the analysis to points along the z axis, as shown in Figure 3, where r, the magnitude of $\mathbf{r}$, is the

same for all magnets on a given ring. It is also assumed that the value for the magnet strength, ϵ_n, is the same for all magnets. In the case of a single ring of six magnets, the gradient of H_x is given by substitution of the values of $\mathbf{m}$ and $\mathbf{r}$ from Table I into Equation 5:

$$\frac{dH_x}{d\mathbf{r}} = -\frac{45\epsilon}{8\pi}\frac{l^3}{r^7}\begin{pmatrix}\sin\phi_o \\ \cos\phi_o \\ 0\end{pmatrix} \quad (6)$$

where l is the radius of the ring of dipoles. Thus a single ring of magnets enables control of the orientation but not the magnitude of the field gradient. To null a quadrupolar term of arbitrary magnitude, a second corrector ring is required. The gradient is given by the sum of the contributions from each ring,

$$\frac{dH_x}{d\mathbf{r}} = --\frac{45\epsilon}{8\pi}l^3\left[\frac{1}{r_1^7}\begin{pmatrix}\sin\phi_{o1} \\ \cos\phi_{o1} \\ 0\end{pmatrix} + \frac{1}{r_2^7}\begin{pmatrix}\sin\phi_{o2} \\ \cos\phi_{o2} \\ 0\end{pmatrix}\right] \quad (7)$$

where r_i ($i = 1,2$) is the distance from the magnets on the ith ring to the point of interest and ϕ_{oi} is the value of odd numbered magnets for the ith ring.

We note a small limitation to consider when chosing the stregth of magnets used for shimming. The gradient has l^3/r^7 dependence. Thus a probe having a finite length in the z dimension will experience a variation in $dH_x/d\mathbf{r}$, even if centered at z_c, the center point between two paired rings. This new inhomogeneity can be minimized by making r as large as possible. Hence, the coil must be centered away from z_c, though this reduces the overall magnitude of gradient that can be produced by the ring pair. The situation is improved with the incorporation of an identical second ring pair symmetrically opposite to the first, as shown in Figure 3. This doubles the available gradient magnitude, whilst further reducing the z-dependence of the H_x gradient. The field gradient at Z_0, the point between the two ring pairs is then simply twice Equation 7.

The ideal case for this system is one where the magnets in Ring 1 and 2 would literally occupy the same space. In this case our rings would be capable of correcting for any field error within the PMs strength in xy up to order 5. It should be noted that Equation 7 implies that there is a minimum gradient magnitude that a given ring pair can correct for. This occurs when $\phi_{o1} = \phi_{o2} + \pi$. To obtain lower magnitude gradients r must be increased by separating the two ring pairs along the z-axis or PMs of smaller strength should be used.

Nulling higher order harmonics can also be done using this system along with using multiple sets of shimming rings for simultaneously nulling multiple orders of harmonics. The corrections for second order and third order inhomogeneities are provided in the Appendix. The PM shims can in principle be used to reduce a z gradient
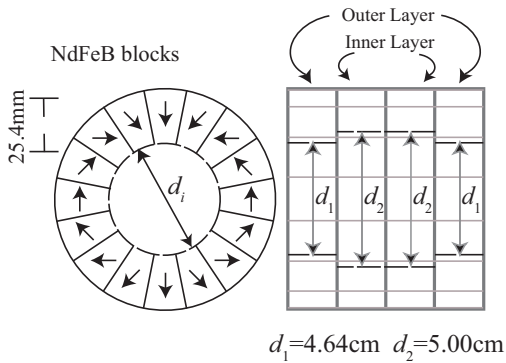
NdFeB blocks

Outer Layer
Inner Layer

25.4mm

d_i

d_1 d_2 d_2 d_1

d_1=4.64cm d_2=5.00cm

FIG. 4: The Halbach array, with four rings having 16 NbFeB elements oriented into a dipole configuration. The outer layers have a radius of 23.2 mm while the inner layers have a radius of 25.0 mm. The strength of the permanent magnet dipole field is about 0.5 T (proton resonance frequency approx. 21.4 MHz

simultaneously with an xy plane gradient through a vectorial superposition of magnet orientations which would individually null the errors in the xy plane and z axis.

III. EXPERIMENT

The magnet is a 16-element NdFeB Halbach array as shown in Figure 4. The elements are arrayed in four layers to produce a dipole field. The array has a mass of approximately 5 kg with an outer diameter of 100 mm and a usable bore diameter of 41 mm. The resulting field stregth was .5T, or a proton resonance frequency of 21.4MHz.

Typical inhomogeneities over a volume of 0.1 mm^3 at the center of the magnet, were approximately 10,500 Hz (450 ppm)(see Figure 7 c). Two types of magnetic inhomogeneities can arise in a magnetic system. One, those produced by the inherent discretization and symmetries of the magnet design. Two, those due to the accuracy of design execution and level of toleration in fabrication. Our magnet described above was designed to have an intrinsic inhomogeneity limit of 20ppm in a field region of 1 mm^3. However, even at this level of homogeneity the field would still benifit from shimming. A third broadening specific in NMR is the field drift, which we will discuss at more length in section IV A.

The shimming experiments were performed on water and flourinated compounds using a Chemagnetics Infinity 400 spectrometer. Due to the significant inhomogeneity in the field, and to bypass the coil ring down time, a single spin echo readout was used to measure the center frequency and linewidth of the peak.

Field measurements were made using a home built probe which consisted of a solenoidal microcoil of length 2 mm and inner diameter 350 μm, using copper wire of width 50 μm, wrapped around a capillary tube of outer diameter 350 μm and inner diameter 250 μm. It was a single resonance probe with the tuning circut located out side of the magnet. This allowed the coil to be on a thin rod which would be movable via a positioning system for accurate field mapping(See Figure 6). The tube was filled with MnCl$_2$ doped water, to keep the T$_1$ relaxation time under 1 second in order to speed up the acquisition time typically to under 2 minutes.

The harmonics correcting device consists of four azimuthally evenly spaced cylindric PMs mounted into rings of Delrin, as shown in Figure 5. The PMs are small cylinders of NdFeB with radius 2.5 mm and length 2 mm. Each PM can be rotated in the xy plane but is prevented from rotation into the z direction. Each ring of PMs is directly adjacent to another ring (Figure 5b and c), in the z axis, creating two pairs. The distance between the two ring pairs can be increased by adding spacers. This reduces the magnitude of the correction gradient, as described at the end of section II B.

Magnetic field maps were constructed from the proton resonance frequency of water (Figure 7a and b) with the mapping coil oriented parallel to the z-axis in order to obtain the smallest possible voxel size in the xy plane. The probe was positioned using a translational stage, as shown in Figure 6, which had a precision of 0.01 mm in all three dimensions.

Using a map of the xy plane of the magnetic field at the Z_0 position, the dominant inhomogeneity in the magnetic field was determined to be a quadrupole, $n = 2$. The values of dH_x/dx and dH_x/dy were determined and used to solve Equation 7 for the angles ϕ_{o1} and ϕ_{o2}. The angles ϕ_{e1} and ϕ_{e2} were calculated from Equation 3 and the PMs were manually oriented into their respective directions.

IV. RESULTS AND DISCUSSION

A. Experiment

Figure 7a and b are maps of the H_x component of the magnetic field before and after placement of the shim rings. The shim rings compensated for a gradient of approximately 2.78 G/mm at 300 degrees with respect to the positive x axis.

In further experiments the nullification of the xy plane, first derivative, gradient was accompanied by a significant improvement in NMR linewidth. In the center region of the magnet, before shimming, linewidths were as great as 12,000 Hz. Figure 7 c) and d) demonstrate the spectroscopic improvement on a water sample. The nullification of the gradient led to a concomitant reduction in half peak width from 10,500 Hz (450 ppm) to 1,200Hz (56 ppm), or an improvement of about 8.75:1. Following the "one-shot" shimming process, linewidth improvements of 7.5:1 were commonplace, whilst improvements of up to 9:1 were sometimes observed. In other experiments, the linewidths of two ^{19}F species were improved to reveal a chemical shift splitting that could otherwise not be resolved, as demonstrated in Figure 7 e) and f).
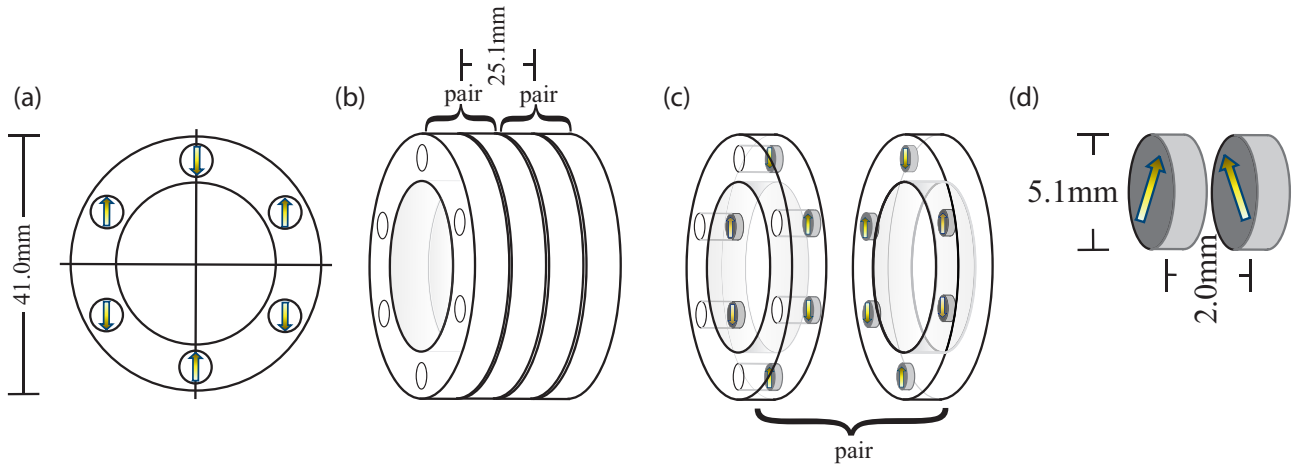
FIG. 5: (a)A face-on view of a single shim ring. Within each ring the PM are equally spaced at angles separated by 60 degrees around the diameter. (b) A pictorial of the two pairs of shims rings used to null a field. The casings for the permanent magnets are white Delrin. From center to center of each pair is 25.1mm. However if the strength of the magnets is too high additional spacers would be added. (c) A single pair of the shims. Within each pair one has the magnet at the base of the casing while the other has them at the top making them adjacent. (d) Each PM has a diameter of 5.1 mm. The centers of permanent magnets pairs are only 2 mm apart, making them close enough to almost null the others field when placed in opposition.
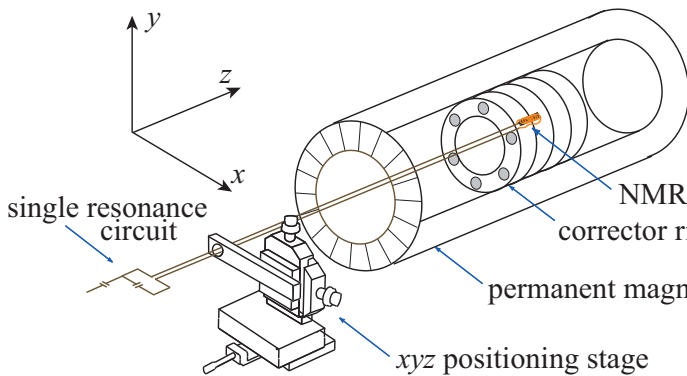

FIG. 6: Total overview of the experimental system showing the PM shim rings within the 16-element Halbach-array magnet. The probe coil is placed close to the shim ring's center and can be precisely positioned using a translational system, allowing for mapping an area of interest in the Halbach-array magnet. Our tuning and matching capasitors are located outside of the magnet so that the coil can have free movement inside the bore of the magnet. The positioner is affixed to the outside of the permanent magnet to ensure that the position is reproducible. Each platform within the positioner has a precision of 0.01 mm.

The gradient in the xy plane was was observed to drift by approximately ± 0.05 G/mm and $\pm 5\,^\circ$ over the course of a day. We determined that, in order to minimize the error introduced by this drift, the field map should be taken and corrector rings inserted within about 60 minutes. However, with temperature stabilization a shim setting could be used for several days. Conveniently, this shimming system has no power supply thus the shims do not warm up causing a more drastic field drift.

Further improvements in linewidth can be made by identifying higher-order inhomogeneities following shimming, and adding additional shim rings to correct for them. Such additional corrections were not necessary in order to resolve the ^{19}F chemical shift in a mixture containing two fluorinated compounds. For higher resolution spectroscopy such as proton NMR, where the whole chemical shift range is 10ppm, this method would be necessary.

B. Error analysis

The shimming magnets are themselves a source of error due to the lack of precision knowledge of the easy-axis orientation and field strength of each PM. The variations in these properties are due to unavoidable inaccuracies in the fabrication process. However, in principle these errors could also be nulled with the system itself. Adjustments of the PM after further inquiries into each PMs properties and further iterations of the mapping, shimming system would eventually allow the system to shim out its own inhomogenieties.

The response of this shimming method to these inaccuracies was analyzed through computer simulation. The computer program used the charge sheet model described by Schlueter et al.[8] to calculate the magnetic field due to the PMs. The PM field strength standard deviation was estimated to be 20 percent while the error in the orientations of the magnets was estimated to be 3 degrees (standard deviation). This variation was included as a random value added or subtracted from the strengths and orientations of the PMs. One hundred simulations
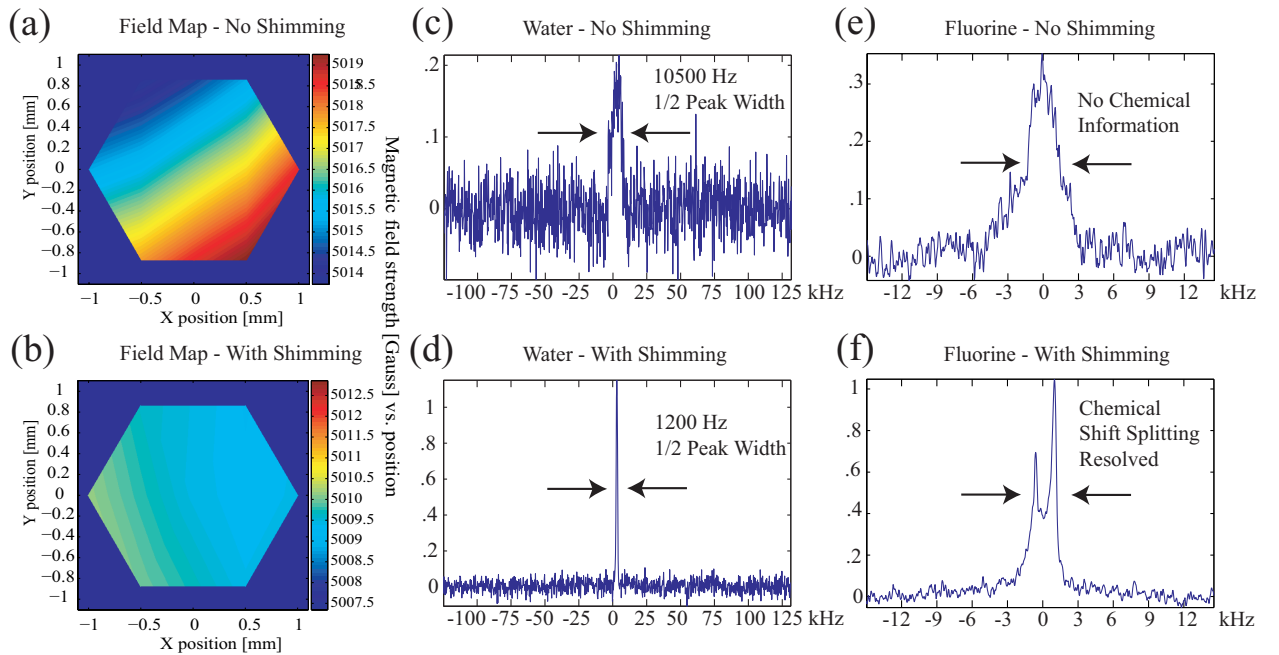
FIG. 7: (a) A field map of the center region of the magnet. Points were taken at even intervals around the circumference of a circle of radius 1 mm, and further data points were taken within the circle. The gradient was determined to be approximately 2.78 G/mm with an orientation of 300 degrees. (b) A field map of the same region following shimming. The gradient was successfully nullified. (c) Spectrum of $MnCl_2$ doped water without shimming after 128 scans. The half peak width is 10,500 Hz (450 ppm). (d) Spectrum of $MnCl_2$ doped water after shimming after 128 scans. The half peak width is 1,200 Hz (56 ppm). This is an 8.75 improvement in linewidth. (e) Spectrum of a mixture of hexa-fluorobenzene and perfluorinated polyether without shimming after 128 scans. No chemical information can be seen. (f) Spectrum of a mixture of hexa-fluorobenzene and perfluorinated polyether with shimming after 128 scans. The chemical shift splitting is clearly resolved.

were run and the data are displayed in Figure 8. From this, we conclude that, within the center of a harmonic corrector ring, a large portion of the area can be used to provide desired gradient corrections.

For a shimming method to be useful, the gradient must be uniform across the spatial extent of the coil. These data imply that the region within center of the magnet has a tolerable variability in its field gradient. This region could be made larger by increasing the accuracy of magnet orientation and improving the consistency of the surface fields of the magnets.

V. CONCLUSION

We have shown that harmonic corrector rings can be used to shim the field of a permanent magnet, leading to NMR linewidth improvements of up to an order of magnitude. Nullification of the quadrupolar inhomogeneity has been demonstrated and the methodology for higher-order harmonics correction using further sets of rings has been outlined. The method has been shown to be robust in response to inherent uncertainties in the strength and orientation of the PMs. Adjustment of the angle and magnitude of the applied correction gradient is simple, allowing for quick response to drift in the magnetic field.

The method could be further sped up by automation of the magnet orientations. The low-cost, simplicity and flexibility of this device make it a useful tool in the development of magnets where field homogeneity is important but shimming coils are unsuitable. In particular, the large size of the usable shimmed region in comparison to the overall size of the corrector rings makes this shimming method particularly convenient for use in small portable NMR systems.

APPENDIX A: HIGHER ORDER GRADIENTS

In general, a ring of n equally spaced permanent magnets can be used to null up to a harmonic of order $n - 1$. Thus the corrector rings described in this paper could be

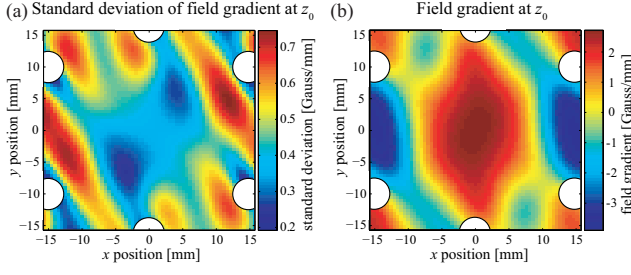(a) Standard deviation of field gradient at z_0 (b) Field gradient at z_0

FIG. 8: The xy coordinates of the PMs, at z_i are projected on the plane of the field map at Z_0, and are indicated by the white circles. The PMs were oriented so that the gradient should be in the $+x$ direction with a magnitude of 2.78 G/mm. (a) Map of the standard deviation of the gradient over the 100 simulations. This map gives a measure of the response of the field gradient to variation in PM orientations and strengths. The standard deviation of the gradient, 2.78 G/mm, in the center region is under 0.4 G/mm. (b) Map of the dH_x/dx component of the mean gradient, with no error in the magnet strengths and orientations. The area where the gradient is within 20 % of the desired gradient at the center comprises a region of about 1/5 the total width of the shim ring.

used to null an inhomogeneity of up to a decapole. The analytical expressions for the second and third derivatives of the field are:

$$
\frac{d^2\mathbf{H}}{d\mathbf{r}^2} = \frac{15}{4\pi r^5}\left[\frac{1}{5}[\mathbf{I}\otimes\mathbf{m} + 2\mathbf{m}\otimes\mathbf{I}] - \hat{\mathbf{r}}\otimes\mathbf{m}\otimes\hat{\mathbf{r}} - \hat{\mathbf{r}}\otimes\hat{\mathbf{r}}\otimes\mathbf{m} \right.
$$
$$
\left. - \mathbf{m}\otimes\hat{\mathbf{r}}\otimes\hat{\mathbf{r}} - (\mathbf{m}\cdot\hat{\mathbf{r}})[\mathbf{I}\otimes\hat{\mathbf{r}} + 2\hat{\mathbf{r}}\otimes\mathbf{I}] + 7(\mathbf{m}\cdot\mathbf{r})\hat{\mathbf{r}}\otimes\hat{\mathbf{r}}\otimes\hat{\mathbf{r}} \right] \tag{A1}
$$

and

$$
\frac{d^3\mathbf{H}}{d\mathbf{r}^3} = \frac{15}{4\pi r^6}\left[7\Big(\mathbf{m}\otimes\hat{\mathbf{r}}\otimes\hat{\mathbf{r}}\otimes\hat{\mathbf{r}} + \hat{\mathbf{r}}\otimes\mathbf{m}\otimes\hat{\mathbf{r}}\otimes\hat{\mathbf{r}} + \hat{\mathbf{r}}\otimes\hat{\mathbf{r}}\otimes\mathbf{m}\otimes\hat{\mathbf{r}} + \hat{\mathbf{r}}\otimes\hat{\mathbf{r}}\otimes\hat{\mathbf{r}}\otimes\mathbf{m} \right.
$$
$$
- 9\,(\mathbf{m}\cdot\hat{\mathbf{r}})\,\hat{\mathbf{r}}\otimes\hat{\mathbf{r}}\otimes\hat{\mathbf{r}}\otimes\hat{\mathbf{r}} + (\mathbf{m}\cdot\hat{\mathbf{r}})\,\hat{\mathbf{r}}\otimes\hat{\mathbf{r}}\otimes\mathbf{I} + 2\,(\mathbf{m}\cdot\hat{\mathbf{r}})\,\mathbf{I}\otimes\hat{\mathbf{r}}\otimes\hat{\mathbf{r}} + 3\,(\mathbf{m}\cdot\hat{\mathbf{r}})\,\hat{\mathbf{r}}\otimes\mathbf{I}\otimes\hat{\mathbf{r}}\Big)
$$
$$
- \hat{\mathbf{r}}\otimes\mathbf{m}\otimes\mathbf{I} - 2\hat{\mathbf{r}}\otimes\mathbf{I}\otimes\mathbf{m} - 2\mathbf{I}\otimes\mathbf{m}\otimes\hat{\mathbf{r}} - 2\mathbf{I}\otimes\hat{\mathbf{r}}\otimes\mathbf{m} - 2\mathbf{m}\otimes\hat{\mathbf{r}}\otimes\mathbf{I}
$$
$$
\left. - 3\mathbf{m}\otimes\mathbf{I}\otimes\hat{\mathbf{r}} - (\mathbf{m}\cdot\hat{\mathbf{r}})\,\mathbf{I}\otimes\mathbf{I} - 2\mathbf{I}\otimes\mathbf{I} \right]. \tag{A2}
$$

Substitution of the terms for the dipole positions from Table II and orientations calculated in Equation 2 yields usable expressions for the second and third derivatives, given in Tables III and IV.

[1] G. Moresi and R. Magin, Concepts Magn. Reson. **19B**, 35 (2003).

[2] H. Raich and P. Blumler, Concepts Magn. Reson. **23B**, 16

TABLE II: The magnet positions, magnetic sextupole vector, and octupole moment vector for the magnets of Figure 1. The ring is determined by the index on z.

| | **r** | | | **m**$/\epsilon$ n=3 | | | **m**$/\epsilon$ n=4 | | |
	r_x	r_y	r_z	m_x	m_y	m_z	m_x	m_y	m_z
1	0	$-l$	$-z_i$	$\cos\theta$	$\sin(\theta+\pi)$	0	$\cos\theta$	$\sin\theta$	0
2	$-\sqrt{3}l/2$	$-l/2$	$-z_i$	$\cos(\theta+4/3\pi)$	$\sin(\theta+4/3\pi)$	0	$\cos(\theta+5/3\pi)$	$\sin(\theta+5/3\pi)$	0
3	$-\sqrt{3}l/2$	$l/2$	$-z_i$	$\cos(\theta+8/3\pi)$	$\sin(\theta+8/3\pi)$	0	$\cos(\theta+10/3\pi)$	$\sin(\theta+10/3\pi)$	0
4	0	l	$-z_i$	$\cos\theta$	$\sin\theta$	0	$\cos(\theta+5\pi)$	$\sin(\theta+5\pi)$	0
5	$\sqrt{3}l/2$	$l/2$	$-z_i$	$\cos(\theta+4/3\pi)$	$\sin(\theta+20/3\pi)$	0	$\cos(\theta+4/3\pi)$	$\sin(\theta+20/3\pi)$	0
6	$\sqrt{3}l/2$	$-l/2$	$-z_i$	$\cos(\theta+8/3\pi)$	$\sin(\theta+25/3\pi)$	0	$\cos(\theta+4/3\pi)$	$\sin(\theta+25/3\pi)$	0

TABLE III: Non-vanishing tensor components of the second derivative $d^2H_x/d^2\mathbf{r}$ calculated from equation A1 through substitution of $\mathbf{r}$ and $\mathbf{m}$ from Table II. Summation over ϕ_n gives the solution for multiple rings.

| indexing | | term |
i	j	times $\frac{45l^2\epsilon_n}{16\pi r^9}$
1	1	$-3\left(7l^2-6r^2\right)\cos\phi_n$
1	2	$\left(7l^2-2r^2\right)\sin\phi_n$
2	1	$\left(7l^2-6r^2\right)\sin\phi_n$
2	2	$-\left(7l^2-10r^2\right)\cos\phi_n$
3	3	$4\left(7l^2-5r^2\right)\cos\phi_n$

TABLE IV: Non-vanishing tensor components of the third derivative $d^3H_x/d^3\mathbf{r}$ calculated from equation A2 through substitution of $\mathbf{r}$ and $\mathbf{m}$ from Table II. Summation over ϕ_n gives the solution for multiple rings.

| indexing | | | term |
i	j	k	times $\frac{15\epsilon_n}{4\pi r^6}$
1	1	1	$\frac{-3\left(16r^6-7l\epsilon_n\left(27l^4+8r^5-12l^2r^2(2+r)\right)\sin\phi_n\right)}{4r^6}$
1	1	2	$\frac{3l\epsilon_n\cos\theta}{r}$
1	2	2	$\frac{-3\left(16r^6-l\epsilon_n\left(63l^4+36r^5-28l^2r^2(3+r)\right)\sin\phi_n\right)}{4r^6}$
1	3	3	$\frac{-3\left(4r^6+l\epsilon_n\left(63l^4-14l^2r^2(6+r)+r^4(28+9)\right)\sin\phi_n\right)}{r^6}$
2	1	1	$\frac{3l\epsilon_n\cos\phi_n}{r}$
2	1	2	$\frac{21l^3\epsilon_n\left(9l^2-4r^3\right)\sin\phi_n}{4r^6}$
2	2	1	$\frac{3l\epsilon_n\left(63l^4+20r^5-28l^2r^2(3+r)\right)\sin\phi_n}{4r^6}$
2	2	2	$\frac{6l\epsilon_n\cos\theta}{r}$
2	3	3	$\frac{3l\epsilon_n\cos\theta}{r}$
3	1	3	$\frac{-21l\epsilon_n\left(9l^4+2r^5-l^2r^2(9+2r)\right)\sin\phi_n}{r^6}$
3	3	1	$\frac{-3l\epsilon_n\left(63l^4+9r^5-14l^2r^2(3+r)\right)\sin\phi_n}{r^6}$
3	3	2	$\frac{3l\epsilon_n\cos\phi_n}{r}$

(2004).

[3] U. Haeberlen, *High resolution NMR in solids, Adv. mag. Reson.* (Academic Press, New York, 1976), suppl. 1 ed.

[4] K. Halbach, Nucl. Instr. Meth. Phys. Res. A **169**, 1 (1980).

[5] C. Meriles, D. Sakellariou, A. Moulè, M. Goldman, T. Budinger, and A. Pines, J. Magn. Reson. **169**, 13 (2004).

[6] D. Sakellariou, C. Meriles, R. Martin, and A. Pines, Chem. Phys. Lett. **377**, 333 (2003).

[7] R. Schlueter, D. Humphries, and J. Tanabe, Nucl. Instr. Meth. Phys. Res. A **395**, 153 (1997).

[8] R. Schlueter and S. Marks, IEEE Trans. Magnetics **32**, 2710 (1996).